Environmental Science & Technology

pubs.acs.org/est

Article

Enhanced Soil Emissions of Reactive Nitrogen Gases by Fertilization and Their Impacts on Secondary Air Pollution in Eastern China

Chuanhua Ren, Xin Huang,* Yanan Wang, Li Zhang, Xueyu Zhou, Weihang Sun, Haoran Zhang, Tengyu Liu, Aijun Ding, and Tao Wang*

Cite This: *Environ. Sci. Technol.* 2025, 59, 5119−5130

Read Online

ACCESS | Metrics & More | Article Recommendations | Supporting Information

ABSTRACT: Nitrogen fertilizer application is accompanied by intense release of multiple reactive nitrogen (Nr) gases such as nitrous acid (HONO), ammonia (NH_3), and nitric oxide (NO) from the soil, influencing atmospheric chemistry and air pollution. In current emission inventories, postfertilization soil emissions are poorly characterized due to inaccurate identification of fertilization timing and location. Moreover, pre-existing studies predominantly focus on individual Nr gases, and a comprehensive understanding of simultaneously emitted Nr gases from fertilization and their impacts on air quality is still limited. Here, we developed a novel method to identify the dryland fertilization activity based on satellite and reanalysis data sets. Then, we updated a dynamic soil Nr emissions model (WRF-SoilN-Chem) with lab-derived parametrization and applied it to analyze the time- and space-varying Nr emissions and their effects on air quality. It is estimated that the Nr emissions from a typical fertilization event in the Yangtze River Delta (YRD) region increased ozone (O_3) and nitrate concentrations by 2.5 and 18.2%, respectively. HONO and NH_3 emissions jointly enhanced nitrate production via gas−particle partitioning. An accurate representation of fertilization and meteorology−emission−chemistry coupled modeling would greatly improve the understanding of the soil Nr emissions and their impacts on regional air pollution.

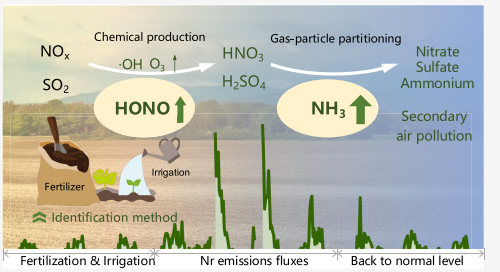

KEYWORDS: *fertilization, irrigation, soil nitrogen emissions, model simulation, air pollution*

1. INTRODUCTION

Agricultural soil emissions are important sources of atmospheric reactive nitrogen (Nr) gases,[1−3] including ammonia (NH_3), nitrous acid (HONO), and nitric oxide (NO), which are produced through various microbial and chemical processes. Nitrogen fertilizer input significantly enhances Nr gases emissions by increasing the soil nitrogen content for microbial activities.[4−6] Field measurements and lab experiments[7−9] show that the Nr gas emissions peak 2−4 days later after fertilization with levels 5−100 times higher than in nonfertilization situations. Such intense Nr emissions, especially NH_3, HONO, and NO, collectively worsen air quality by contributing to the formation of tropospheric ozone (O_3) and particulate matter (PM) via different chemical pathways.[10−16]

A variety of soil Nr emissions models,[17−19] including WRF-CMAQ-EPIC[20] (NH_3), WRF-SoilN-Chem[21] (NH_3), Yienger and Levy (YL)[22] (NO), Model of Emissions of Gases and Aerosols from Nature (MEGAN)[23] (NO), and Berkley-Dalhousie Iowa Soil NO Parameterization (BDISNP)[24] (NO), have been developed and applied to investigate the role of soil Nr emissions in air quality. Sha et al.[25] revealed the impacts of soil NO emissions on O_3 in rural California with the BDISNP model. Wang et al.[26] demonstrated that soil HONO emissions aggravate O_3 and nitrate pollution in northern China by WRF-CMAQ coupled with HONO parametrization. Pleim et al.[20] evaluated the NH_3 emitted from fertilized croplands and grasslands in North America with the WRF-CMAQ-EPIC model. These models are effective in the assessment of individual Nr gases species. However, in real agricultural fields, multiple gases are released concurrently after fertilization. A recent study assesses the impact of soil HONO and NO emissions on O_3 and nitrate in a nonfertilization month.[27] So far, there has been little discussion on the simultaneous Nr gas emissions from fertilization and their collective impacts on air quality.

Another challenge in fertilization relevant studies arises from the coarse or inaccurate fertilization spatiotemporal information, which is attributable to the irregularity of farmlands and diverse cultivation practices of smallholder farmers in China.[28,29] As Nr surging emissions appear 2−4 days after fertilization, exact dates and location of fertilization are critical for soil emissions analysis. The pre-existing studies typically obtain fertilization information from crop calendars or surveys of local farmers.[30−32] However, crop calendars with a temporal

Received: November 10, 2024
Revised: February 19, 2025
Accepted: February 20, 2025
Published: March 7, 2025

resolution of 1−2 months are insufficiently detailed to accurately capture surging soil emissions lasting for only 1−2 weeks. Furthermore, the questionnaire method is labor-intensive and time-consuming, particularly in large agricultural regions, such as the North China Plain (NCP) and the Yangtze River Delta (YRD).

In this work, we aim to clarify the impact of fertilization Nr emissions on regional air quality using a novel approach to identify daily dryland fertilization and an updated emissions model incorporating dynamic soil NO, HONO, and NH_3 parametrization. We chose the YRD, which has extensive and fertile croplands, as a case study region to apply this new approach and model for analysis. The results indicate that the intense Nr emissions during a typical fertilization activity noticeably enhance the ambient oxidizing capacity and promote nitrate formation. This work advances the understanding of the effects of fertilization-induced Nr emissions on air pollution, emphasizing the need for considering agricultural emissions in future air quality strategies.

2. MATERIALS AND METHODS

2.1. Identification Method of Fertilization Events. In light of the limitation concerning fertilization spatiotemporal information, we propose a novel method for identifying fertilization events in drylands based on multiple data sets, including the crop calendar, land use, satellite soil moisture measurements, and reanalysis data of soil moisture. This methodology is mainly based on two key features in crop cultivation practices.

First, fertilization and irrigation are typically carried out concurrently during the sowing season. In modern cultivation practices, farmers usually drill the fertilizer together with seeds to optimize labor efficiency and subsequently irrigate the fertilized soil immediately (within approximately 30 min)[33,34] to facilitate the fertilizer hydrolysis and maintain soil moisture for seed germination.[35] In regions with a higher mechanization level like the NCP or YRD, farmers adopt the water-fertilization integration (WFI) technique that mixes fertilizer with water and delivers the mixture to soil through a pipe or pressure system to supply nutrients directly to the crop.[36] Such synchronicity between the two processes makes it reasonable to identify fertilization events through irrigation occurrence.

Second, the disparity of soil moisture dry−wet transition trends between satellite and reanalysis data can serve as an indicator of irrigation activities. Satellite observations directly detect soil brightness temperature and calculate soil moisture.[37,38] Thus, both natural rainfall and irrigation-induced soil wetting can be detected by the satellite measurements.[39] However, unlike direct measurements by satellite, reanalysis data are generated by combining historical observations with model outputs using data assimilation techniques. This process assimilates precipitation but does not incorporate human activities like irrigation; hence, reanalysis data cannot represent irrigation-induced soil wetting.[40,41] Therefore, a daily comparison between satellite observations and reanalysis data on different areas can identify the timing and location of irrigation. The concurrency of fertilization and irrigation makes it possible to derive the spatiotemporal distribution of fertilization with a spatial resolution of 25 km, following the soil moisture data resolution.

This identification method is suitable for most dryland crops but has limitations on wetland crops such as rice and taro and other semiaquatic crops, where the reliability of the satellite retrievals is far lower than that in drylands.[42] Though this method is applicable to basal fertilization during the planting season, it may not be feasible during the growing season, when irrigation and fertilization can be conducted separately. As dryland constitutes the majority of China's cropland (i.e., 75.45%)[43] and the basal fertilization accounts for 63% of the total fertilizer consumption for dryland crops,[44] this method is thus applicable under most cultivation situations in China.

2.2. Implementation of Soil HONO and NO Emissions in WRF-SoilN-Chem. WRF-SoilN-Chem is a dynamic soil Nr emissions model coupled with meteorology−chemistry transport model WRF-Chem, capable of numerically describing the agriculture Nr emissions rate interactively with time- and spatial-varying meteorological and soil conditions. In the original version of WRF-SoilN-Chem, the dynamic fertilization NH_3 emission flux is obtained by multiplying static basic emissions (Basic $E(NH_3)$) with dynamic emission correction factors (CF), as shown in eq 1 and eq 2. The descriptions of the model parametrization and evaluation are detailed by Ren et al.[21]

$$\mathrm{flux}_{\mathrm{NH3-fertilizer}} = \mathrm{Basic}\ E(\mathrm{NH_3})_{\mathrm{fertilizer}} \times \mathrm{CF}_{\mathrm{wind}} \times \mathrm{CF}_{\mathrm{soilT}} \times \mathrm{CF}_{\mathrm{soilm}} \times \mathrm{CF}_{\mathrm{rain}} \quad (1)$$

$$\mathrm{EF}_{\mathrm{static}_{\mathrm{fertilizer}}} = \mathrm{EF}_{0\mathrm{i}} \times \mathrm{CF}_{\mathrm{pH}} \times \mathrm{CF}_{\mathrm{method}} \times \mathrm{CF}_{\mathrm{rate}} \times \mathrm{CF}_{\mathrm{time}} \quad (2)$$

where $\mathrm{flux}_{\mathrm{NH3-fertilizer}}$ (mol km^{-2} h^{-1}) is the dynamic NH_3 emission flux from fertilization. Basic $E(NH_3)_{\mathrm{fertilizer}}$ (mol km^{-2} h^{-1}) is the basic NH_3 emission flux from fertilization, which is calculated from the nitrogen fertilizer rate multiplied by the static emission factor ($\mathrm{EF}_{\mathrm{static}_{\mathrm{fertilizer}}}$) at a specific condition. $\mathrm{CF}_{\mathrm{wind}}$, $\mathrm{CF}_{\mathrm{soilT}}$, $\mathrm{CF}_{\mathrm{soilm}}$, and $\mathrm{CF}_{\mathrm{rain}}$ are the dynamic meteorological correction factors (CF) for wind speed, soil temperature, soil moisture content, and rainfall, respectively. $\mathrm{EF}_{0\mathrm{i}}$ is the reference emission factor for different nitrogen fertilizers. $\mathrm{CF}_{\mathrm{pH}}$ is the correction factor for different soil acidities; $\mathrm{CF}_{\mathrm{method}}$ is for the fertilization application method, including basal dressing and top dressing; $\mathrm{CF}_{\mathrm{rate}}$ is for different application rates, and $\mathrm{CF}_{\mathrm{time}}$ is for time since fertilizer application, which is used to reflect the variation characteristics of NH_3 emission after fertilization. The detailed parametrizations of these CF are described in the Table S1.

In this work, we updated the model by incorporating additional soil HONO and NO emissions based on Oswald et al.,[45] Zhang et al.,[46] and Wang et al.[26] Given the substantial differences in Nr gas emissions before and after fertilization, we classified agricultural soil emissions into two states: the postfertilization state and the background state. Since Nr emissions usually peak 2−4 days after fertilization and return to the nonfertilization level within 10 days, the postfertilization state is defined as "within 10 days after fertilizer application". The background state is defined as "before fertilization" or "10 days later after fertilization" time, when Nr emissions are at a low level.

For HONO emission in the background state, Oswald et al.[45] estimated HONO optimum emission ($F_{\mathrm{N,opt}}$) from different soil samples like forest, pasture, grassland, wheat, and cotton fields. The optimum soil HONO flux is scaled by the function of soil temperature (T) and soil water content (SWC); based on laboratory experiments, the parametrization is eq 3:

https://doi.org/10.1021/acs.est.4c12324
Environ. Sci. Technol. 2025, 59, 5119−5130

$$F_{SHONO} = F_{N,opt} \times h(T) \times g(SWC) \quad (3)$$

where $F_{N,opt}$ is the optimum flux of HONO in terms of N mass (ng N m^{-2} s^{-1}). $h(T)$ is a dimensionless function of HONO emissions with respect to soil T, and $g(SWC)$ is the function of HONO emissions on SWC (% water-holding capacity (WHC)).

For HONO emissions in the postfertilization state, we utilized the fertilization parametrization of Wang et al.[26] to represent the enhanced HONO emissions after fertilization within 10 days. The postfertilization HONO emissions (F_{SHONO}) are predicted as a function of soil temperature and SWC in eq 4. The detailed equation method and parameters can be found in Wang et al.'s work:[26]

$$\begin{aligned} F_{SHONO} &= F_{emis(HONO)}(\text{dry peak}) + F_{emis(HONO)}(\text{wet peak}) \\ &= [F_{N,max_{dry}} \cdot \exp(-\frac{(SWC - SWC_{C_{dry}})^2}{w_{dry}^2}) \\ &\quad + F_{N,max_{wet}} \cdot \exp(-\frac{(SWC - SWC_{C_{wet}})^2}{w_{wet}^2})] \\ &\quad \times \exp[(-\frac{43{,}900}{R}) \cdot (\frac{1}{T} - \frac{1}{298})] \end{aligned} \quad (4)$$

F_{emis}(dry peak) is the fitted Gaussian function in the low SWC range (0−60% WHC) and F_{emis}(wet peak) is in the high SWC range (60−100% WHC), $F_{N,max}$ is the maximum HONO flux at the optimum SWC ($SWC_{C_{Wet/dry}}$) at the reference temperature of 298 K, and w characterizes the width of the curves. The dry and wet subscripts represent the parameters on the dry peak and wet peak, respectively. R is the gas constant (8.314 J mol^{-1} K^{-1}).

Given that the default WRF-Chem model includes only one pathway for HONO formation via the hydroxyl radical (OH) and NO, we integrated additional sources, including vehicle emissions and secondary pathways (Tables S2 and S3), to enhance the accuracy of HONO concentration estimation and assess the contributions of postfertilization to HONO.

For NO, the background and postfertilization soil NO emission schemes are from Wang et al.[27] and Wang et al.,[26] respectively. In these schemes, the NO flux is calculated based on the maximum NO flux under optimum conditions ($F_{N,max}$(NO)) and further adjusted by the soil water content and soil temperature, similar to the approach used for HONO. The NO parametrization equation (eq 5) follows the same form as the HONO equation. The difference lies in the value of parameters such as $F_{N,max_{Dry}}$, $F_{N,max_{wet}}$, $SWC_{C_{Wet}}$, $SWC_{C_{dry}}$, w_{Wet}, and w_{Dry}, which are derived from the curve fitting of HONO and NO flux data. The specific values of these parameters are provided in Table S4.

$$\begin{aligned} F_{NO} &= F_{emis(NO)}(\text{dry peak}) + F_{emis(NO)}(\text{wet peak}) \\ &= [F_{N,max_{dry}} \cdot \exp(-\frac{(SWC - SWC_{C_{dry}})^2}{w_{dry}^2}) \\ &\quad + F_{N,max_{wet}} \cdot \exp(-\frac{(SWC - SWC_{C_{wet}})^2}{w_{wet}^2})] \\ &\quad \times \exp[(-\frac{43{,}900}{R}) \cdot (\frac{1}{T} - \frac{1}{298})] \end{aligned} \quad (5)$$

Since the measured HONO and NO emissions may include contributions from each other due to the oxidation of NO to HONO, as well as the rapid photolysis of HONO to NO, Wang et al.[26] placed the entire sampling setup inside a dark cabinet and dried the soil with purified air throughout the experiment to minimize the transformation between HONO and NO and obtain more accurate measurements. Given that the diagnosed model includes individual chemical reaction processes, such explicit HONO and NO soil emissions in the atmospheric chemistry model are essential for providing detailed diagnosis and quantification of the impacts on air quality.

2.3. Model Configuration and Simulation Design. To evaluate the model performance of the updated WRF-SoilN-Chem and the air quality response to soil Nr emissions, we designed six parallel experiments: base, HONO, NH_3, NO, NH_3+HONO, and NH_3+HONO+NO. The base experiment applied the anthropogenic emission inventory for 2020 from the Multiresolution Emission Inventory for China (MEIC)[47,48] but excluded the fertilization and soil emissions of all Nr gases. Other sensitivity experiments were conducted by introducing additional soil Nr emissions into the base experiment, as detailed in Table 1. We adopt fertilizer application of 100 kg N

Table 1. Simulation Experiment Design Considering Different Sources of Soil Nr Emissions

	additional fertilization emissions considered		
experiments	soil HONO	soil NH_3	soil NO
base	×	×	×
HONO	√	×	×
NH_3	×	√	×
NO	×	×	√
NH_3+HONO	√	√	×
NH_3+HONO+NO	√	√	√

ha^{-1} during the identified basal fertilization stage, following the fertilization rate statistics in the YRD provided by Zhang et al.[49] To investigate fertilization Nr emission and its impact on air quality during the whole time period of the identified fertilization event (see Section 3.2), simulations are conducted from 20 Sep to 10 Oct 2021, with the first 10 days as a spin-up time. The model domain covers eastern China (18° N−50° N, 95° E−131° E) with a 20 km grid resolution. Other key settings are detailed in Text S1 and Table S5. The simulations of key surface meteorological parameters and pollutants are validated by available observations in Figures S1−S3. The normalized mean biases of temperatures, RH, and wind speed in Nanjing are −3.6, 1.7, and 35.9%, respectively. The simulation well captures the spatial pattern and pollution level of $PM_{2.5}$, CO, O_3, NO_2, nitrate, and ammonium concentrations measured by surface stations in the YRD (Figures S2 and S3).

As mentioned in Section 2.1, the reanalysis data could not accurately simulate irrigation-induced soil wetting. Since soil moisture directly affects soil emissions simulation, we used satellite-detected moisture to drive the simulation. Based on the method from Lee et al.,[50] we assimilated the satellite soil moisture retrievals at 00 UTC in all experiments.

2.4. Identification of Potential Air Mass Source Regions. The Lagrangian particle dispersion modeling (LPDM) was conducted using the hybrid single-particle Lagrangian integrated trajectory model (HYSPLIT) driven

https://doi.org/10.1021/acs.est.4c12324
Environ. Sci. Technol. 2025, 59, 5119−5130

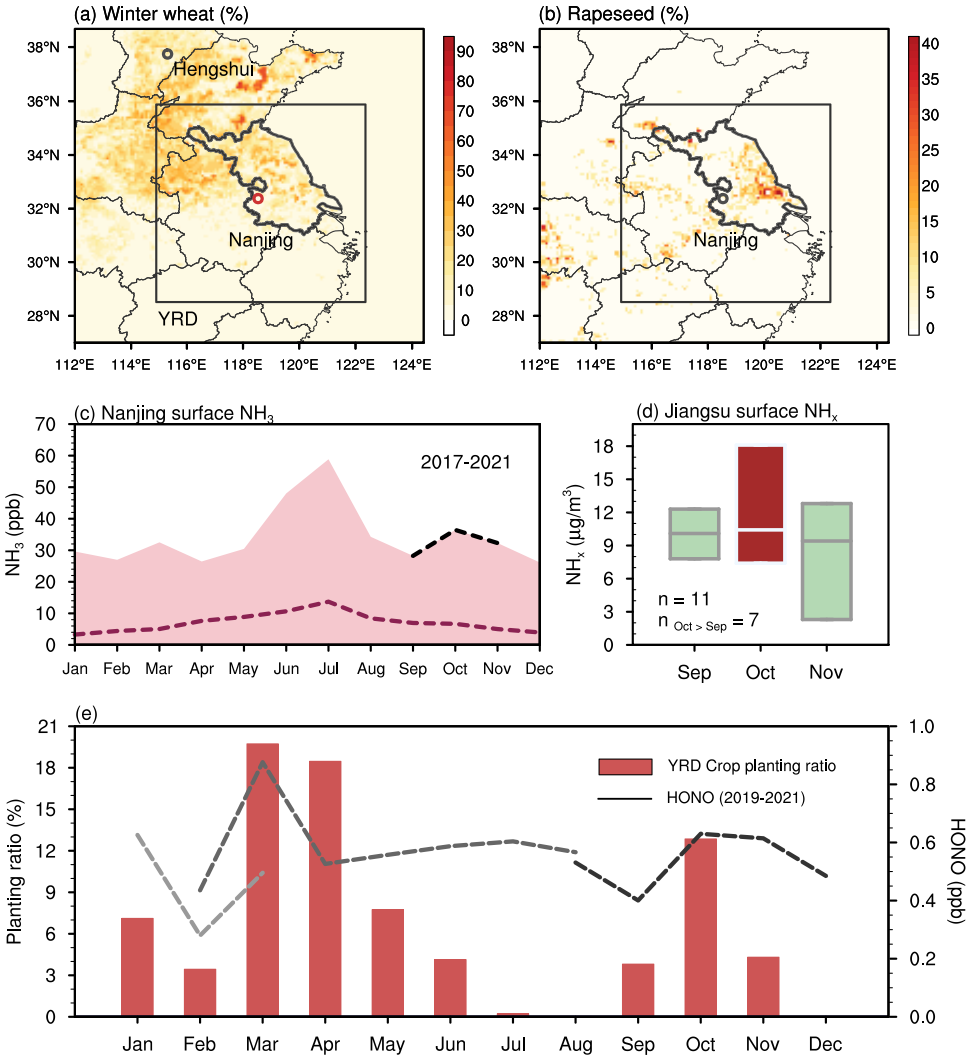

Figure 1. Observational evidence of the effects of fertilization on Nr concentrations. Percentage of (a) winter wheat and (b) rapeseed coverage[62] at a 20 m resolution in the YRD region (black box); the black thick line outlines the Jiangsu province. (c) Averaged NH_3 concentration in the Nanjing SORPES site during 2017−2021; the upper and lower edges of the filled area are 99 and 1%, respectively. (d) Mean surface NH_x (NH_3(gas) + NH_4^+(aerosol)) concentration of the YRD region sites from 2011 to 2015 according to the nationwide nitrogen deposition monitoring network (NNDMN) data set;[63] *n* is the count of valid value. (e) YRD seasonal crop planting ratio and HONO concentration in Nanjing.

by Global Data Assimilation System (GDAS) to identify the potential sources of air masses during the studied pollution case.[51] The LPDM was run in the 24 h backward mode, with 3000 particles released every 2 h over the Nanjing station. Particle residence times below 100 m were used to identify the "footprint" of air masses arriving at the Nanjing station. The spatiotemporal distributions of these particles were used to identify potential source regions and their relative contributions to air masses at the Nanjing station.

2.5. Data Sets. *2.5.1. In Situ Measurements.* Hourly concentrations of NH_3, HONO, O_3, nitrogen dioxide (NO_2), carbon monoxide (CO), sulfur dioxide (SO_2), and $PM_{2.5}$ were measured at the Station for Observing Regional Processes of the Earth System (SORPES, 32°07′14′ N, 118°57′10′ E; ∼40 masl) in Nanjing, Jiangsu province. NH_3 concentrations were measured with a Picarro G2103 gas analyzer (Picarro, Inc., USA) that employs a cavity ring-down spectroscopy (CRDS) technique.[52] HONO concentrations were measured using a commercial long-path absorption photometer instrument (LOPAP).[53] NO_x, O_3, and CO were measured by Thermo Fisher analyzers (TEI 42i, 49i, and 48i, USA, respectively). The $PM_{2.5}$ concentrations were detected using a mass analyzer (Thermo SHARP-5030). Furthermore, aerosol components, including sulfate (SO_4^{2-}), nitrate (NO_3^-), and ammonium (NH_4^+) were measured by a Monitor for Aerosols and Gases in ambient Air (MARGA).

In addition to the data from SORPES, hourly $PM_{2.5}$, SO_2, NO_2, O_3, and CO data from other YRD stations were obtained from China's Air Quality Monitoring Network.[54] The meteorological observations, including wind, temperature, precipitation, and relative humidity, were obtained from the National Climatic Data Center's (NCDC) Integrated Surface Database (ISD).

2.5.2. Soil Moisture Data Sets. Soil moisture observations from the satellite were obtained using the Advanced Microwave Scanning Radiometer−Earth Observing System and version 2 (AMSR−E/AMSR2) instruments. Previous assessments have shown that the AMSR instruments are highly sensitive to changes in soil moisture, whether they're caused by rainfall or irrigation.[39] This sensitivity is reflected in the strong correlation between satellite and aircraft soil moisture measurements, both spatially (average R = 0.92 and RMSD

https://doi.org/10.1021/acs.est.4c12324
Environ. Sci. Technol. 2025, 59, 5119−5130

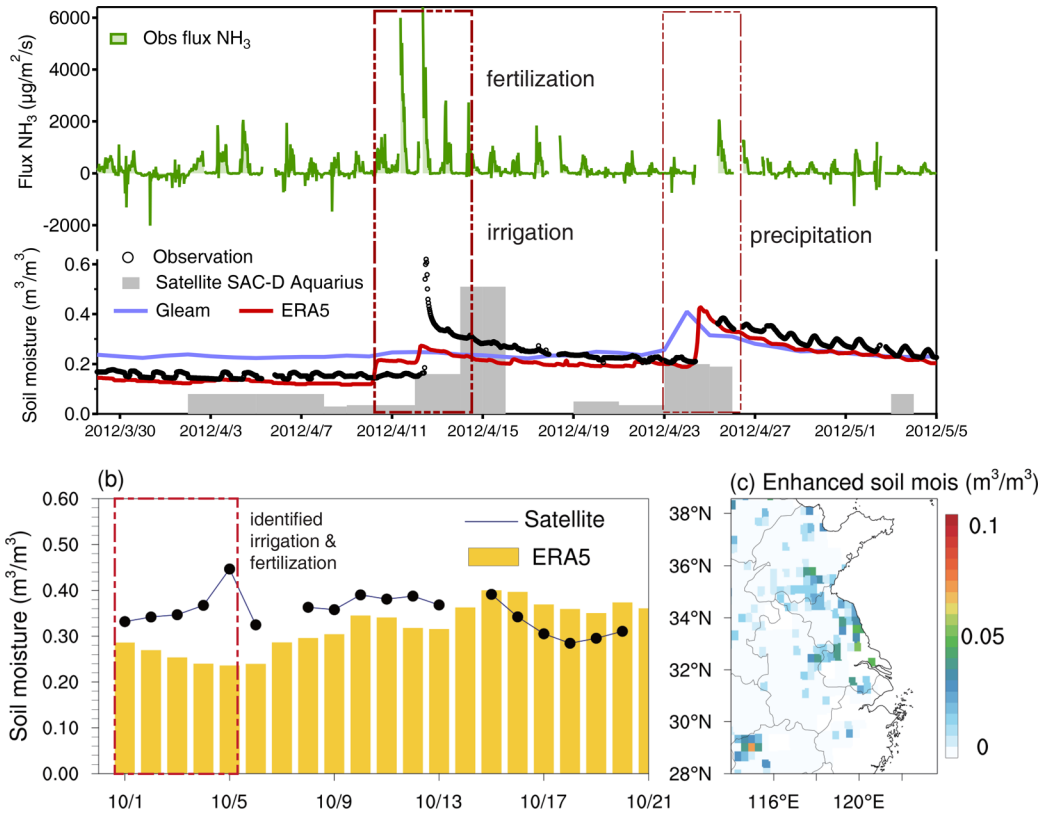

Figure 2. Identification of the timing and location of a fertilization and irrigation event. (a) Time series of the observed ammonia flux and moisture in Hengshui farmland, Hebei province of China. The gray bar refers to the soil moisture from satellite SAC-D Aquarius, and the purple and red lines are the GLEAM and ERA5 reanalysis data sets, respectively. The black circle markers indicate the field measurements. (b) Daily satellite-detected and ERA5 soil moisture on Jiangsu croplands in October 2021, and the bounding red box represents the identified irritation and fertilization dates. (c) Enhanced soil moisture from Oct 1 to Oct 5, 2021.

= 0.049 m^3 m^{-3}) and over time (R = 0.94 and RMSD = 0.04 m^3 m^{-3}).[55] The data provided by this product cover a 25 × 25 km^2 area and are updated daily, making it a valuable resource for monitoring soil conditions.

The hourly soil moisture reanalysis data used in this study are from ECMWF Reanalysis v5 (ERA5).[56] ERA5 assimilates precipitation data from the Tropical Rainfall Measuring Mission Microwave Imager (TRMM−MI) and demonstrated outstanding soil moisture dynamic properties in past evaluations.[57]

2.5.3. Crop Planting Data Sets. The planting day of crops in the YRD region is obtained from the Global Gridded Crop Model Intercomparison (GGCMI) Phase 3 data set.[58] It provides in each 0.5° land grid cell the planting day and maturity day for 18 different crops, separating rainfed and irrigated systems. To represent the crop planting intensity in different seasons, we calculate the crop planting ratio in each month as follows:

$$\text{planting ratio}_{(m)}(\%) = \frac{F_{(m)}}{\sum_{m=1}^{12} F_{(m)}} = \frac{\sum_i \sum_j \sum_c N_{(c,i,j,m)}}{\sum_m \sum_i \sum_j \sum_c N_{(c,i,j,m)}} \quad (6)$$

where c represents the crop type, m denotes the month in a year, and i and j are the location indices of the data grid. N indicates the planting event, where N = 1 means a planting event occurs, and N = 0 otherwise. $F_{(m)}$ is the frequency of planting events in each month calculated by summing the planting events for each crop type, each grid, and each day within the month.

3. RESULTS AND DISCUSSION

3.1. Enhanced HONO and NH_3 Concentration during the Fertilization Period. The YRD region, covering approximately 126,505 km^2 of cultivated land (9.3% of the national cultivated land area), features the most fertile soil in China[59] and is highly suitable conditions for crop farming. Rice, wheat, and rapeseed are the main economic crops grown in the YRD region.[60] Rice is the staple crop distributed across most areas of the YRD region, whereas winter wheat and rapeseed are mainly cultivated in northern (Figure 1a) and eastern YRD region (Figure 1b), respectively. According to the crop calendar, early rice and spring corn are sown from March to April, and winter wheat and rapeseed are predominantly planted in October. Therefore, the crop planting seasons in the YRD are mainly concentrated in March, April, and October (Figure 1e).

Intensive agricultural crop cultivation makes the YRD a hot spot region for agricultural Nr gas emissions.[61] Persistently extensive planting activities accompanied by fertilization lead to substantial locally emitted Nr pollutants, and thus, ambient Nr concentrations and crop planting ratio exhibit similar peaking time in the planting season. Multiyear observations (2017−2021) from the Nanjing SORPES station showed that

https://doi.org/10.1021/acs.est.4c12324
Environ. Sci. Technol. 2025, 59, 5119−5130

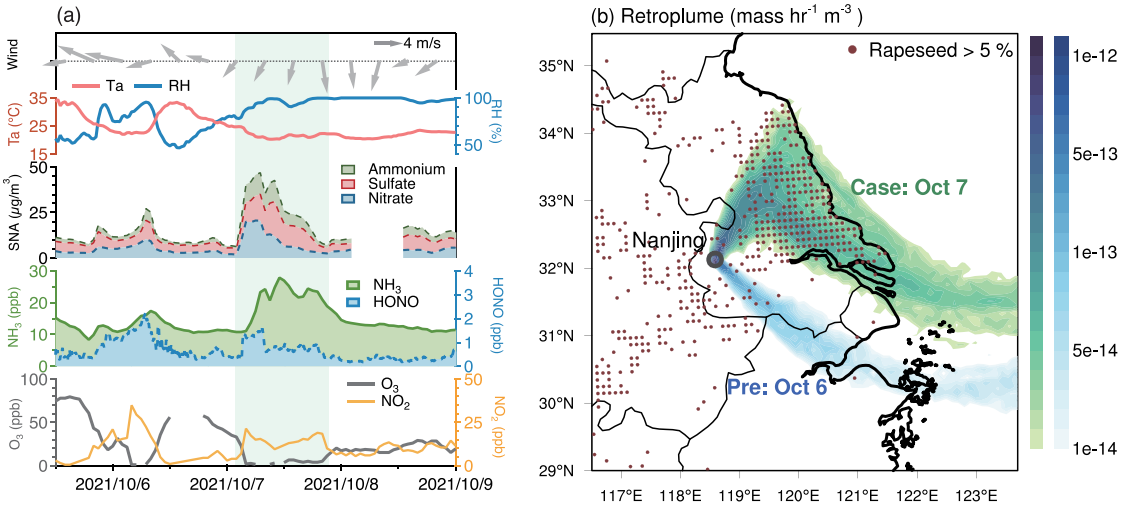

Figure 3. Typical air pollution episode and the potential impact from agricultural sources. (a) Time series of meteorological parameters (air temperature (Ta), relative humidity (RH), and wind) and the concentrations of NH_3, HONO, O_3, NO_2, and ammonium, sulfate, and nitrate at the SORPES station in Nanjing during October 5−9, 2021. The pollution period is marked by the green box. (b) 24 h backward retroplume of Nanjing on clean day Oct 6 (blue) and polluted day Oct 7 (green). The brown dots represent the agricultural fields with more than 5% rapeseed planting.

the average HONO, the maximum NH_3 concentration, and the crop planting ratio peaked in January, March, and October (Figure 1c,e). The Pearson correlation coefficient between Nr concentrations and the planting ratio is 0.58. Besides Nanjing, other rural sites (for example, Fengyang in Anhui province and Fenghua in Zhejiang province) in the YRD exhibited a similar phenomenon of higher Nr concentrations in the sowing season (Figure 1d). As clearly demonstrated in Figure 1d and Figure S4, the substantial enhancement of both ground and satellite observed NH_3 in October (the sowing month) compared to that in September (the warmer month) indicates a more important role of fertilization than warmer temperature in Nr emissions.

3.2. Postfertilization Soil Nr Emissions and Their Regional Transport. By evaluating the method in Section 2.1 and applying it to identify a typical fertilization event in the YRD, we can investigate the postfertilization effects on air quality. Previous field measurements of postfertilization fluxes in the YRD region have supported our identification method with observations of the simultaneous increase in Nr emissions and soil moisture following fertilization and irrigation during the sowing period.[64,65] The high-resolution field measurements conducted by our research group in a crop field in Hengshui city (Hebei province of China) provide another opportunity to verify our identification method. As shown in Figure 2a, during the corn planting season (April 2012), as farmers applied fertilizer and irrigated the soil, both the NH_3 emission flux and soil moisture simultaneously increased by 4−6 times on April 12. The soil moisture from satellite observations and reanalysis data showed different dry−wet transitions by the irrigation. Specifically, the soil moisture from the SAC-D (Satélite de Aplicaciones Científicas) satellite effectively captures the dry−wet transition caused by irrigation and rainfall events on April 12 and April 24, respectively. However, the Global Land Evaporation Amsterdam Model (GLEAM) and ERA5, which exclusively assimilate precipitation, can only indicate a soil moisture increase due to rainfall on April 24. In short, the combination of the satellite and reanalysis data is able to distinguish the fertilization event.

Considering the noisy performance of satellite data on waterlogged paddy fields, we examined the bare drylands sown with wheat and rapeseed in October in the YRD region. Figure 2b shows different temporal trends between ERA5 reanalysis and the AMSR satellite data sets in early October. The satellite-observed soil moisture increased continuously from October 1 to 5, while the ERA5 value remained stable. The Integrated MultisatellitE Retrievals for Global Precipitation Measurement (IMERG) (Figure S5) shows no precipitation during this period, suggesting that the soil wetting was dominantly caused by irrigation. As displayed in Figure 2c, the soil wetting was most pronounced in eastern and northern Jiangsu provinces, overlapping with the wheat and rapeseed cultivation areas, further confirming the occurrence of irrigation and fertilization. Besides this observational evidence, the official guidelines from the Ministry of Agriculture and Rural Affairs recommend early October (Oct 1−10) as the optimum time for sowing and fertilizing winter wheat and rapeseed in the "Huaihe River Basin" and "Yangtze-Huaihe region"[66] in 2021. The above analyses confirm the occurrence of fertilizer application from October 1 to 5, and they support the feasibility of the proposed method for determining the timing and location of fertilization.

An air pollution episode occurring 2 days after the extensive fertilization showed a plausible connection to fertilization-related nitrogen emissions. As shown in Figure 3a, on the morning of Oct 7, high levels of HONO, NH_3, sulfate, nitrate, and ammonium (SNA) with the prevailing northerly wind were recorded in the Nanjing SORPES station. The pollution episode lasted for 1 day with maximum NH_3 reaching up to 30 ppb, which was 5 times higher than that in the clean state. The satellite retrieval also demonstrated the NH_3 hot spot in Jiangsu province on Oct 7 (Figure S6). As agricultural activity is the major source of NH_3, the sudden rise in pollutant concentrations accompanied by a change in the wind direction indicated that both agricultural emissions and regional transport are probable causes of this pollution event.

The Goddard Earth Observing System (GEOS) model with assimilation showed that nitrate and sulfate pollution was partly transported from North and South Korea to Nanjing

https://doi.org/10.1021/acs.est.4c12324
Environ. Sci. Technol. 2025, 59, 5119−5130

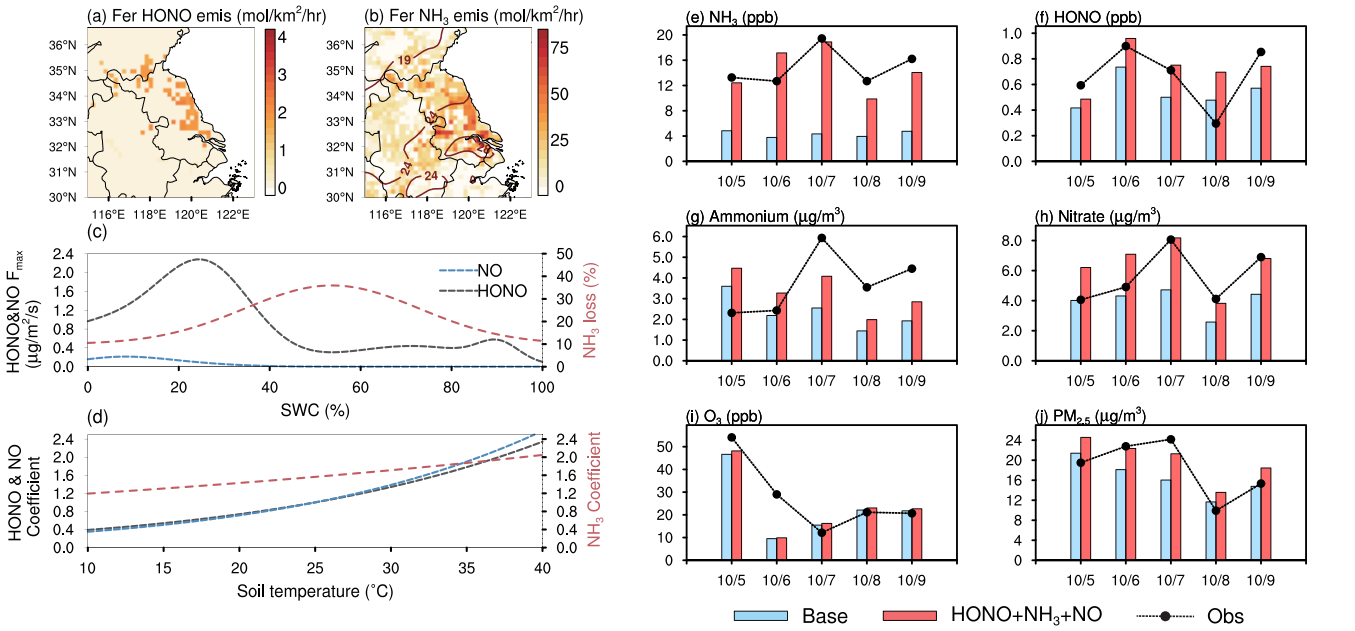

Figure 4. Improved model performance on air quality by including fertilization Nr emissions. Spatial distribution of simulated (a) HONO and (b) NH_3 fertilization emissions and soil temperature (isolines in unit of °C) during the case period (October 1−10). Sensitivity of Nr emissions to (c) soil water content (SWC) and (d) soil temperature. (e−j) Daily observed (black line) and simulated (blue and red bars) NH_3, HONO, ammonium, nitrate, and O_3 and $PM_{2.5}$ concentration in Nanjing during the pollution episode.

along with the northerly wind (Figure S7). The base experiment without postfertilization was able to reproduce the rise of nitrate concentration caused by such regional transport but still obviously underestimated it (Figure S8), indicating the missing of potential sources. Source attribution based on LPDM showed that the air mass on the polluted (October 7) day originated from the ocean and passed through the extensively fertilized rapeseed plots (Figure 3b). Along the transport pathway, the upstream soil-emitted Nr gases were carried to Nanjing, contributing to the observed increase in fine particle pollution, particularly ammonia and associated secondary aerosols.

The lifetime of ammonia is approximately 12 h,[67] and our calculations indicate that such a lifetime is sufficiently long for NH_3 emitted from the farthest Jiangsu fields to be transported to Nanjing. In comparison, noontime HONO is short-lived (10−20 min) and originates from various sources, including traffic emissions and heterogeneous reactions. Due to its rapid photolysis, HONO emitted during the daytime from eastern Jiangsu is unlikely to reach Nanjing SORPES via long-range transport. Only emissions from nearby farmlands can contribute to HONO levels observed at the SORPES station. However, the HONO emitted from distant farmlands can contribute to the formation of longer-lived pollutants such as O_3 or SNA, which exert broader and prolonged effects.[68]

3.3. Quantifying Fertilized Soil Nr Emissions and Their Impacts on Air Pollution. To investigate the impacts of fertilization emissions on air quality, we performed diagnosed simulations with an air quality model incorporating dynamic soil Nr emissions (WRF-SoilN-Chem, see methods). In the YRD region, the simulated emissions of NH_3 and HONO (Figure 4a,b) and NO (Figure S9) during the postfertilization period (October 1−10) were 28.5, 1.09, and 0.19 mol km^{-2} h^{-1}, respectively, in good agreement with the Nr flux measured by Zhao et al.,[69] Xia et al.,[64] and Wang et al.[27] in the YRD (Table S6). The spatial patterns of these Nr emissions show notable heterogeneity across different species. For HONO and NO, emissions were concentrated in the eastern and northern parts of Jiangsu, where soil moisture was elevated (~30% WHC) after irrigation (Figure S10). For NH_3, high emissions are concentrated not only in eastern and northern Jiangsu but also in southern Jiangsu. This spatial heterogeneity can be attributed to their distinct sensitivities to soil moisture and soil temperature. According to the Nr emission parametrizations, the NH_3 emission peaks at 50% WHC,[70] the HONO peaks at 25% and 90% WHC, and the NO peaks at 10% WHC (Figure 4c). Thus, the irrigated soil moisture conditions (~30% WHC) are more favorable for peak HONO emissions to occur. Under the same soil temperature, the NH_3 emission factor is larger than HONO (Figure 4d).[71,72] During the case period, the soil temperature in the southern Jiangsu was 7−9 °C higher than that in the northern part. Such a high temperature led to a substantial increase in NH_3 emissions in the southern region, resulting in regional heterogeneity in Nr emissions.

The fertilization Nr emissions significantly improved the simulation of relevant pollutants in the Nanjing SORPES site during the pollution period (Figure 4e−j and Figure S11). Agricultural NH_3 emissions from upstream regions improved the simulation of NH_3 in Nanjing, in both magnitude and temporal variation (Figure 4e). As an alkaline gas, NH_3 can react with ambient sulfuric acid (H_2SO_4) and nitric acid (HNO_3) to form $(NH_4)_2SO_4$, NH_4HSO_4, and NH_4NO_3 aerosols; hence, the enhanced NH_3 also mitigates the underestimation of NH_4^+, NO_3^-, and $PM_{2.5}$ (Figure S12). The base experiment revealed a slight underestimation of HONO compared to NH_3 (Figure 4f), indicating that local nonagricultural sources dominate HONO production at SORPES (Figure S13a). Despite this, additional soil HONO emissions contributed to elevated nitrate and $PM_{2.5}$ concentrations (Figure S12). In contrast, soil NO emissions were

https://doi.org/10.1021/acs.est.4c12324
Environ. Sci. Technol. 2025, 59, 5119−5130

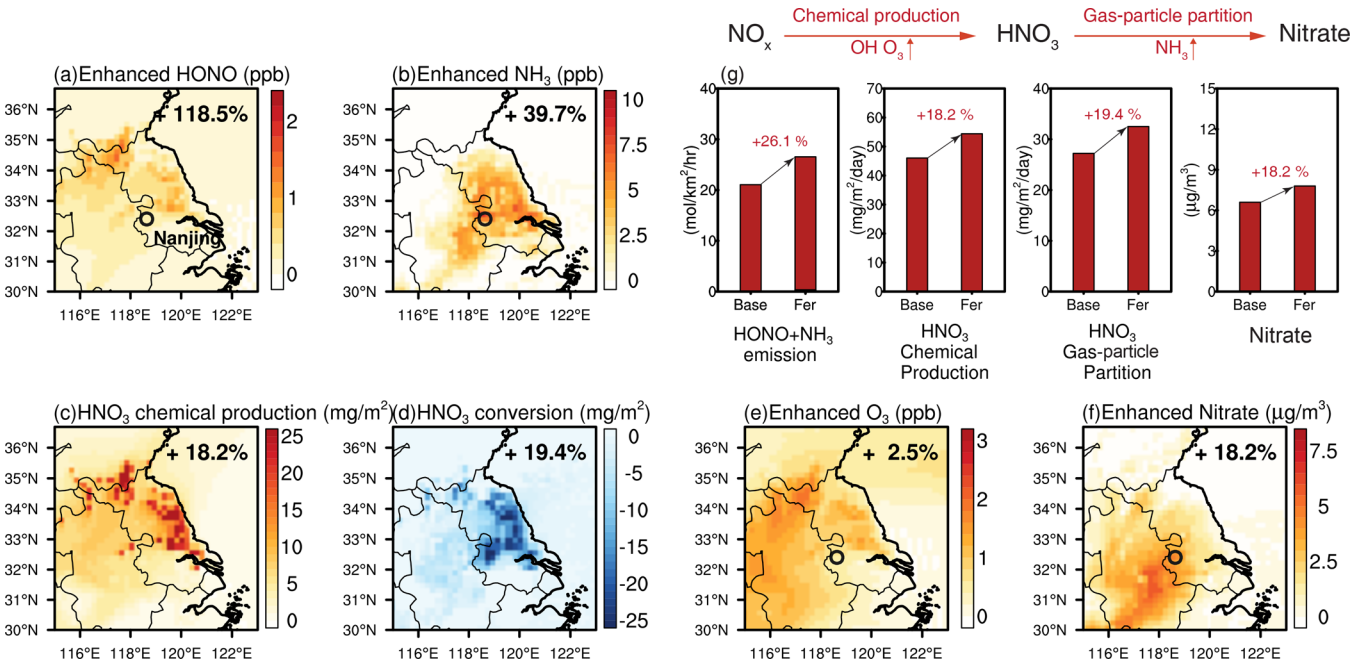

Figure 5. Impacts of soil Nr emissions after fertilization on the concentration of O_3 and secondary aerosol pollution in the YRD region. Distribution of enhanced (a) HONO, (b) NH_3, (c) HNO_3 chemical production, (d) HNO_3 gas−particle conversion, (e) O_3, and (f) nitrate concentration by fertilization Nr emissions during October 1−10, 2021. (g) Key processes and factors driving the formation of O_3 and nitrate in the map area.

negligible relative to HONO and NH_3, resulting in a minimal effect on air quality in this case (Figure S14).

To quantitatively understand the enhanced secondary pollution by soil Nr emissions, we identified the chemical processes in the YRD region. As shown in Figure 5, with fertilization emissions, the average simulated HONO and NH_3 mixing ratio in the YRD region increased by 0.5 ppb (118.5%) and 5.9 ppb (39.7%), respectively. The photolysis of HONO is an important source of atmospheric OH that regulates atmospheric oxidizing capacity and the production of secondary pollutants, such as O_3. Along with the enhanced HONO, OH and O_3 also increased by 11.0% (Figure S13b) and 2.5% (Figure 5e), respectively. Diagnostic analysis showed that such an enhanced atmospheric oxidizing capacity facilitates the formation of HNO_3 by accelerating the chemical conversion of NO_x to HNO_3 (Figure 5c). Moreover, the soil-emitted NH_3 facilitates HNO_3 gas−particle conversion by neutralizing HNO_3 gas, thus facilitating particulate NO_3^- formation (Figure 5d). The increased emissions of HONO and NH_3 each play a dominant role in the two major steps required for NO_3^- production, collectively contributing to the overall production of nitrate (Figure 5g). Thus, sensitivity experiments showed that the joint effects of HONO and NH_3 emissions on nitrate formation are larger than the sum of the individual impacts (Figure S12). Such a nonlinear response of the nitrate formation is mainly caused by thermodynamic equilibrium as detailed in Text S2. This single fertilization event resulted in a 18.2% increase in nitrate concentrations in YRD, demonstrating the significance of crop fertilization in Nr emissions and regional air pollution.

The responses of nitrate production show great regional disparities depending on its chemical sensitivity to NH_3 or HNO_3 according to the thermodynamic equilibrium principle.[14,73] For the YRD region, where the nitrate formation regime is mainly NH_3-limited,[74] increasing NH_3 alone significantly enhanced nitrate formation (Figures S16 and S17). In addition, the secondary formation of sulfate can also be influenced by the presence of NH_3. For instance, the rate of sulfate formation pathways like aqueous-phase oxidation of SO_2 by NO_2, O_3, and Mn-catalyzed oxidation on aerosol surfaces, are positively correlated to aerosol pH.[75] In the NH_3-limited regime, the aerosol pH notably increased with excess NH_3 due to lower aqueous H^+ concentrations,[76] likely resulting in a higher sulfate formation rate during this pollution event.

Though fertilization-induced emissions of nitrogen-containing trace gases are dynamically depicted in this work, some limitations and uncertainties need further efforts. In our simulations, it is assumed that all fields within a single grid applied fertilizer on the same day, which might not be that realistic and thus introduces some biases in emission estimation. Furthermore, our simulations only considered fertilizer emissions from drylands, which means that the impact of soil emissions on air quality could be even greater while taking other agricultural land types (e.g., rice paddies) into account. Additionally, the rewetting of soils through rainfall or irrigation can trigger nitrogenous gas emissions (the Birch effect),[77−79] which was not accounted for in our simulations. Despite these limitations, our results clearly demonstrate the significant influence and spatial heterogeneity of agricultural emissions on air quality and the necessity of including them in air quality modeling.

4. IMPLICATIONS

We developed a novel fertilization identification method and a dynamic emission model to access soil Nr emissions and their combined impacts on air pollution in China, with a specific focus on the agriculture-intensive YRD region. Compared to the widely used monthly emission rates based on static statistics, the updated agricultural emission estimation in this

https://doi.org/10.1021/acs.est.4c12324
Environ. Sci. Technol. 2025, 59, 5119−5130

work is capable of depicting high-resolution Nr emissions by pinpointing fertilization activities and considering time- and spatial-varying meteorological and soil conditions. When coupled with the air quality model, dynamic NH_3 and HONO emissions would more accurately capture the day-to-day variability in the ambient concentration of $PM_{2.5}$ and O_3 precursors. Such dynamic emission and its coupling with air quality model could shed more light on the role of fertilization in regional air quality, particularly during the postfertilization period. Our simulations show that Nr emissions from a typical fertilization event collectively contribute to a 2.5% increase in ozone concentrations and a 18.2% enhancement in nitrate levels over the YRD region. As China's pollutant emissions controls have been relatively stringent for the industrial and transportation sectors in the past decade, the impacts of soil emissions on the nitrogen cycle and atmospheric environment are expected to be increasingly prominent, especially during the fertilization period. Given that there are no specific regulations and standards for controlling emissions of air pollutants from agricultural activities currently, it is of great urgency to investigate the impacts of agricultural emissions on air pollution and to incorporate them into future air quality improvement strategies. Additionally, there is a need for more comprehensive and accurate data regarding agricultural management, such as the fertilizer application rate, timing, and types and locations of fertilizer uses, which are essential for developing effective models and making informed and cost-effective decisions. By addressing these research gaps, more targeted strategies to mitigate the adverse effects of agriculture on air quality could be achieved.

■ ASSOCIATED CONTENT

Supporting Information

The Supporting Information is available free of charge at https://pubs.acs.org/doi/10.1021/acs.est.4c12324.

> Detailed parametrized HONO source mechanisms included in the model; explanation of methods and modeling parameters employed; data quality control and model evaluation with observed air pollutants and meteorological elements; simulated daily average soil water content distribution in Jiangsu; model-simulated impacts of soil NH_3, HONO, and NO emissions after fertilization in the YRD region (PDF)

■ AUTHOR INFORMATION

Corresponding Authors

Xin Huang − *Joint International Research Laboratory of Atmospheric and Earth System Sciences, School of Atmospheric Sciences, Nanjing University, Nanjing 210023, China; Jiangsu Provincial Collaborative Innovation Center for Climate Change, Nanjing 210023, China;* orcid.org/0000-0003-0922-5014; Email: xinhuang@nju.edu.cn

Tao Wang − *Department of Civil and Environmental Engineering, Hong Kong Polytechnic University, Hong Kong 99907, China*; Email: tao.wang@polyu.edu.hk

Authors

Chuanhua Ren − *Department of Civil and Environmental Engineering, Hong Kong Polytechnic University, Hong Kong 99907, China; Joint International Research Laboratory of Atmospheric and Earth System Sciences, School of Atmospheric Sciences, Nanjing University, Nanjing 210023, China*

Yanan Wang − *Department of Civil and Environmental Engineering, Hong Kong Polytechnic University, Hong Kong 99907, China*

Li Zhang − *California Air Resources Board, Riverside, California 92507, United States*

Xueyu Zhou − *Joint International Research Laboratory of Atmospheric and Earth System Sciences, School of Atmospheric Sciences, Nanjing University, Nanjing 210023, China*

Weihang Sun − *Department of Civil and Environmental Engineering, Hong Kong Polytechnic University, Hong Kong 99907, China*

Haoran Zhang − *Joint International Research Laboratory of Atmospheric and Earth System Sciences, School of Atmospheric Sciences, Nanjing University, Nanjing 210023, China*

Tengyu Liu − *Joint International Research Laboratory of Atmospheric and Earth System Sciences, School of Atmospheric Sciences, Nanjing University, Nanjing 210023, China; Jiangsu Provincial Collaborative Innovation Center for Climate Change, Nanjing 210023, China;* orcid.org/0000-0002-3137-5898

Aijun Ding − *Joint International Research Laboratory of Atmospheric and Earth System Sciences, School of Atmospheric Sciences, Nanjing University, Nanjing 210023, China; Jiangsu Provincial Collaborative Innovation Center for Climate Change, Nanjing 210023, China;* orcid.org/0000-0003-4481-5386

Complete contact information is available at: https://pubs.acs.org/10.1021/acs.est.4c12324

Notes

The authors declare no competing financial interest.

■ ACKNOWLEDGMENTS

The authors would like to acknowledge Zhen Wang, Liangyu Wei, and Xingzhao Sun for providing farmers' practices and agricultural management information and acknowledge Yuliang Liu and Tao Xu for the maintenance of the data instrument. This research was supported by the Hong Kong Research Grants Council (T24-504/17-N), the Ministry of Science and Technology of the People's Republic of China (2022YFC3701105), and the Postgraduate Research & Practice Innovation Program of Jiangsu Province (KYCX24_0204).

■ REFERENCES

(1) Yang, B.; Zhang, T.; Zhang, M.; Li, B. Reactive Nitrogen Releases and Nitrogen Footprint during Intensive Vegetable Production Affected by Partial Human Manure Substitution. *Environ. Sci. Pollut Res.* **2022**, *29* (13), 19572−19582.

(2) Su, H.; Cheng, Y.; Oswald, R.; Behrendt, T.; Trebs, I.; Meixner, F. X.; Andreae, M. O.; Cheng, P.; Zhang, Y.; Pöschl, U. Soil Nitrite as a Source of Atmospheric HONO and OH Radicals. *Science* **2011**, *333* (6049), 1616−1618.

(3) Lu, X.; Ye, X.; Zhou, M.; Zhao, Y.; Weng, H.; Kong, H.; Li, K.; Gao, M.; Zheng, B.; Lin, J.; Zhou, F.; Zhang, Q.; Wu, D.; Zhang, L.; Zhang, Y. The Underappreciated Role of Agricultural Soil Nitrogen Oxide Emissions in Ozone Pollution Regulation in North China. *Nat. Commun.* **2021**, *12* (1), 5021.

(4) Bhattarai, H. R.; Wanek, W.; Siljanen, H. M. P.; Ronkainen, J. G.; Liimatainen, M.; Hu, Y.; Nykänen, H.; Biasi, C.; Maljanen, M.

Denitrification Is the Major Nitrous Acid Production Pathway in Boreal Agricultural Soils. *Commun. Earth Environ* **2021**, *2* (1), 1−10.
(5) Delon, C.; Galy-Lacaux, C.; Serça, D.; Loubet, B.; Camara, N.; Gardrat, E.; Saneh, I.; Fensholt, R.; Tagesson, T.; Le Dantec, V.; Sambou, B.; Diop, C.; Mougin, E. Soil and Vegetation-Atmosphere Exchange of NO, NH3, and N2O from Field Measurements in a Semi Arid Grazed Ecosystem in Senegal. *Atmos. Environ.* **2017**, *156*, 36−51.
(6) Luo, L.; Cohan, D. S.; Gurung, R. B.; Venterea, R. T.; Ran, L.; Benson, V.; Yuan, Y. Impacts Assessment of Nitrification Inhibitors on U.S. Agricultural Emissions of Reactive Nitrogen Gases. *Journal of Environmental Management* **2024**, *359*, No. 121043.
(7) Xue, C.; Ye, C.; Zhang, C.; Catoire, V.; Liu, P.; Gu, R.; Zhang, J.; Ma, Z.; Zhao, X.; Zhang, W.; Ren, Y.; Krysztofiak, G.; Tong, S.; Xue, L.; An, J.; Ge, M.; Mellouki, A.; Mu, Y. Evidence for Strong HONO Emission from Fertilized Agricultural Fields and Its Remarkable Impact on Regional O3 Pollution in the Summer North China Plain. *ACS Earth Space Chem.* **2021**, *5* (2), 340−347.
(8) Oikawa, P. Y.; Ge, C.; Wang, J.; Eberwein, J. R.; Liang, L. L.; Allsman, L. A.; Grantz, D. A.; Jenerette, G. D. Unusually High Soil Nitrogen Oxide Emissions Influence Air Quality in a High-Temperature Agricultural Region. *Nat. Commun.* **2015**, *6* (1), 8753.
(9) Pan, S. Y.; He, K. H.; Liao, Y. L. Fertilization-Induced Reactive Nitrogen Gases and Carbon Dioxide Emissions: Insight to the Carbon-Nitrogen Cycles. *Sustainable Environ. Res.* **2023**, *33* (1), 23.
(10) Xue, C.; Ye, C.; Lu, K.; Liu, P.; Zhang, C.; Su, H.; Bao, F.; Cheng, Y.; Wang, W.; Liu, Y.; Catoire, V.; Ma, Z.; Zhao, X.; Song, Y.; Ma, X.; McGillen, M. R.; Mellouki, A.; Mu, Y.; Zhang, Y. Reducing Soil-Emitted Nitrous Acid as a Feasible Strategy for Tackling Ozone Pollution. *Environ. Sci. Technol.* **2024**, *58* (21), 9227−9235.
(11) Luo, L.; Ran, L.; Rasool, Q. Z.; Cohan, D. S. Integrated Modeling of U.S. Agricultural Soil Emissions of Reactive Nitrogen and Associated Impacts on Air Pollution, Health, and Climate. *Environ. Sci. Technol.* **2022**, *56* (13), 9265−9276.
(12) Emmanouil, C.; Drositi, E.; Vasilatou, V.; Diapouli, E.; Krikonis, K.; Eleftheriadis, K.; Kungolos, A. Study on Particulate Matter Air Pollution, Source Origin, and Human Health Risk Based of PM10 Metal Content in Volos City. *Greece. Toxicological & Environmental Chemistry* **2017**, *99* (4), 691−709.
(13) Oprea, M.; Dunea, D.; Liu, H.-Y. Development of a Knowledge Based System for Analyzing Particulate Matter Air Pollution Effects on Human Health. *Environmental engineering and management journal* **2017**, *16*, 669−676.
(14) Seinfeld, J. H.; Pandis, S. N. *Atmospheric Chemistry and Physics: From Air Pollution to Climate Change*. 2016, 3rd ed. John Wiley: Hoboken, NJ, pp 412−414.
(15) Wang, Y.; Zhang, Q. Q.; He, K.; Zhang, Q.; Chai, L. Sulfate-Nitrate-Ammonium Aerosols over China: Response to 2000−2015 Emission Changes of Sulfur Dioxide, Nitrogen Oxides, and Ammonia. *Atmospheric Chemistry and Physics* **2013**, *13* (5), 2635−2652.
(16) Liu, M.; Huang, X.; Song, Y.; Tang, J.; Cao, J.; Zhang, X.; Zhang, Q.; Wang, S.; Xu, T.; Kang, L.; Cai, X.; Zhang, H.; Yang, F.; Wang, H.; Yu, J. Z.; Lau, A. K. H.; He, L.; Huang, X.; Duan, L.; Ding, A.; Xue, L.; Gao, J.; Liu, B.; Zhu, T. Ammonia Emission Control in China Would Mitigate Haze Pollution and Nitrogen Deposition, but Worsen Acid Rain. *Proc. Natl. Acad. Sci. U. S. A.* **2019**, *116* (16), 7760−7765.
(17) Val Martin, M.; Blanc-Betes, E.; Fung, K. M.; Kantzas, E.; Kantola, I.; Chiaravalloti, I.; Taylor, L.; Emmons, L.; Wieder, W.; Planavsky, N.; Masters, M.; DeLucia, E.; Tai, A.; Beerling, D. Improving Nitrogen Cycling in a Land Surface Model (CLM5) to Quantify Soil N 2 O, NO, and NH 3 Emissions from Enhanced Rock Weathering with Croplands. *Geoscientific Model Development* **2023**, *16*, 5783−5801.
(18) Fung, K. M.; Val Martin, M.; Tai, A. Modeling the Interinfluence of Fertilizer-Induced NH3 Emission, Nitrogen Deposition, and Aerosol Radiative Effects Using Modified CESM2. *Biogeosciences* **2022**, *19*, 1635−1655.
(19) Li, B.; Chen, L.; Shen, W.; Jin, J.; Wang, T.; Wang, P.; Yang, Y.; Liao, H. Improved Gridded Ammonia Emission Inventory in China. *Atmospheric Chemistry and Physics* **2021**, *21* (20), 15883−15900.
(20) Pleim, J. E.; Ran, L.; Appel, W.; Shephard, M. W.; Cady-Pereira, K. New Bidirectional Ammonia Flux Model in an Air Quality Model Coupled With an Agricultural Model. *Journal of Advances in Modeling Earth Systems* **2019**, *11* (9), 2934−2957.
(21) Ren, C.; Huang, X.; Liu, T.; Song, Y.; Wen, Z.; Liu, X.; Ding, A.; Zhu, T. A Dynamic Ammonia Emission Model and the Online Coupling with WRF−Chem (WRF−SoilN−Chem v1.0): Development and Regional Evaluation in China. *Geosci. Model Dev.* **2023**, *16* (6), 1641−1659.
(22) Yienger, J. J.; Levy, H., II Empirical Model of Global Soil-Biogenic NOχ Emissions. *Journal of Geophysical Research: Atmospheres* **1995**, *100* (D6), 11447−11464.
(23) Guenther, A. B.; Jiang, X.; Heald, C. L.; Sakulyanontvittaya, T.; Duhl, T.; Emmons, L. K.; Wang, X. The Model of Emissions of Gases and Aerosols from Nature Version 2.1 (MEGAN2.1): An Extended and Updated Framework for Modeling Biogenic Emissions. *Geoscientific Model Development* **2012**, *5* (6), 1471−1492.
(24) Hudman, R. C.; Moore, N. E.; Mebust, A. K.; Martin, R. V.; Russell, A. R.; Valin, L. C.; Cohen, R. C. Steps towards a Mechanistic Model of Global Soil Nitric Oxide Emissions: Implementation and Space Based-Constraints. *Atmospheric Chemistry and Physics* **2012**, *12* (16), 7779−7795.
(25) Sha, T.; Ma, X.; Zhang, H.; Janechek, N.; Wang, Y.; Wang, Y.; Castro García, L.; Jenerette, G. D.; Wang, J. Impacts of Soil NOx Emission on O3 Air Quality in Rural California. *Environ. Sci. Technol.* **2021**, *55* (10), 7113−7122.
(26) Wang, Y.; Fu, X.; Wu, D.; Wang, M.; Lu, K.; Mu, Y.; Liu, Z.; Zhang, Y.; Wang, T. Agricultural Fertilization Aggravates Air Pollution by Stimulating Soil Nitrous Acid Emissions at High Soil Moisture. *Environ. Sci. Technol.* **2021**, *55* (21), 14556−14566.
(27) Wang, Y.; Fu, X.; Wang, T.; Ma, J.; Gao, H.; Wang, X.; Pu, W. Large Contribution of Nitrous Acid to Soil-Emitted Reactive Oxidized Nitrogen and Its Effect on Air Quality. *Environ. Sci. Technol.* **2023**, *57* (9), 3516−3526.
(28) Jin, J.; Wu, R.; Liu, R. Rice Production and Fertilization in China. *Better Crops Int.* **2002**, *16*, 26−29.
(29) Sun, X.; Ritzema, H.; Huang, X.; Bai, X.; Hellegers, P. Assessment of Farmers' Water and Fertilizer Practices and Perceptions in the North China Plain. *Irrigation and Drainage* **2022**, *71* (4), 980−996.
(30) *Crop Calendar Charts*. https://ipad.fas.usda.gov/ogamaps/cropcalendar.aspx (accessed 2023−12−12).
(31) *Survey shows how — and when — farmers use fertilizer*. https://www.farmprogress.com/crops/survey-shows-how-and-when-farmers-use-fertilizer (accessed 2024−01−29).
(32) Crotty, F.; McCalman, H.; Powell, H.; Buckingham, S.; Marley, C. Should Farmers Apply Fertilizer According to When Their Daffodils Are in Flower? Utilizing a "Farmer-Science" Approach to Understanding the Impact of Soil Temperature on Spring N Fertilizer Application in Wales. *Soil Use and Management* **2019**, *35* (1), 169−176.
(33) *Notice of the General Office of the Ministry of Agriculture on issuing the Implementation Plan for Promoting the Integration of Water and Fertilizer (2016−2020)*. http://www.moa.gov.cn/nybgb/2016/diwuqi/201711/t20171127_5920793.htm (accessed 2024−06−21).
(34) *Integration of water and fertilizer in China Agricultural Technical Services Manual*. http://www.jsgg.com.cn/Files/PictureDocument/20170216122923179831343060.pdf (accessed 2024−06−21).
(35) Follmer, C. M.; Hummes, A. P.; Lângaro, N. C.; Petry, C.; Moterle, D. F.; Bortoluzzi, E. C. Nutrient Availability and pH Level Affect Germination Traits and Seedling Development of Conyza Canadensis. *Sci. Rep* **2021**, *11* (1), 15607.
(36) Liao, Q.; Nie, J.; Yin, H.; Luo, Y.; Shu, C.; Cheng, Q.; Fu, H.; Li, B.; Li, L.; Sun, Y.; Chen, Z.; Ma, J.; Li, N.; Zhang, X.; Yang, Z. Can the Integration of Water and Fertilizer Promote the Sustainable

https://doi.org/10.1021/acs.est.4c12324
Environ. Sci. Technol. 2025, 59, 5119−5130

Development of Rice Production in China? *Agriculture* **2024**, *14* (4), 585.
(37) ADEOS-II *AMSR Soil Moisture Algorithm*. https://www.eorc.jaxa.jp/AMSR/satellite/pdf.adeos-ii/alg_des.pdf (accessed 2024−06−21).
(38) Reichle, R. H.; Jackson, T.; Kimball, J.; Koster, R. D. *Soil Moisture Active Passive (SMAP) Project Assessment Report for the Beta-Release L4_SM Data Product*.National Aeronautics and Space Administration, Goddard Space Flight Center, 2015
(39) Draper, C. S.; Walker, J. P.; Steinle, P. J.; de Jeu, R. A. M.; Holmes, T. R. H. An Evaluation of AMSR−E Derived Soil Moisture over Australia. *Remote Sensing of Environment* **2009**, *113* (4), 703−710.
(40) Lal, P.; Singh, G.; Das, N. N.; Colliander, A.; Entekhabi, D. Assessment of ERA5-Land Volumetric Soil Water Layer Product Using In Situ and SMAP Soil Moisture Observations. *IEEE Geosci. Remote Sensing Lett.* **2022**, *19*, 1−5.
(41) Martens, B.; Miralles, D. G.; Lievens, H.; van der Schalie, R.; de Jeu, R. A. M.; Fernández-Prieto, D.; Beck, H. E.; Dorigo, W. A.; Verhoest, N. E. C. GLEAM v3: Satellite-Based Land Evaporation and Root-Zone Soil Moisture. *Geoscientific Model Development* **2017**, *10* (5), 1903−1925.
(42) Sakai, T.; Iizumi, T.; Okada, M.; Nishimori, M.; Grünwald, T.; Prueger, J.; Cescatti, A.; Korres, W.; Schmidt, M.; Carrara, A.; Loubet, B.; Ceschia, E. Varying Applicability of Four Different Satellite-Derived Soil Moisture Products to Global Gridded Crop Model Evaluation. *International Journal of Applied Earth Observation and Geoinformation* **2016**, *48*, 51−60.
(43) *third national land resource survey*. http://agri.china.com.cn/2021-08/27/content_41656841.htm (accessed 2024−02−11).
(44) Wang, J.; Ma, W.; Jiang, R.; Zhang, F. Analysis about Amount and Ratio of Basal Fertilizer and Topdressing Fertilizer on Rice, Wheat, Maize in China. *Chin. J. Soil Sci.* **2008**, *39* (2), 329−333.
(45) Oswald, R.; Behrendt, T.; Ermel, M.; Wu, D.; Su, H.; Cheng, Y.; Breuninger, C.; Moravek, A.; Mougin, E.; Delon, C.; Loubet, B.; Pommerening-Röser, A.; Sörgel, M.; Pöschl, U.; Hoffmann, T.; Andreae, M. O.; Meixner, F. X.; Trebs, I. HONO Emissions from Soil Bacteria as a Major Source of Atmospheric Reactive Nitrogen. *Science* **2013**, *341* (6151), 1233−1235.
(46) Zhang, L.; Wang, T.; Zhang, Q.; Zheng, J.; Xu, Z.; Lv, M. Potential Sources of Nitrous Acid (HONO) and Their Impacts on Ozone: A WRF-Chem Study in a Polluted Subtropical Region: MODELING HONO IN A SUBTROPICAL REGION. *J. Geophys. Res. Atmos.* **2016**, *121* (7), 3645−3662.
(47) Li, M.; Liu, H.; Geng, G.; Hong, C.; Liu, F.; Song, Y.; Tong, D.; Zheng, B.; Cui, H.; Man, H.; Zhang, Q.; He, K. Anthropogenic Emission Inventories in China: A Review. *National Science Review* **2017**, *4* (6), 834−866.
(48) *MEICModel − Tracking Athropogenic Emissions in China*. http://meicmodel.org.cn/#firstPage (accessed 2023−12−12).
(49) Zhang, Z.; Dong, L.; Liu, P.; Zhou, T.; Sun, L. Nitrogen Flow Characteristics of Agricultural Production and Consumption System in the Yangtze River Delta Region and Its Driving Factors. *Environ. Sci.* **2024**, *45* (9), 5451−5463.
(50) Lee, J. A.; Jiménez, P. A.; Kumar, R.; He, C. Impact of Direct Insertion of SMAP Soil Moisture Retrievals in WRF-Chem for Dust Storm Events in the Western U.S. *Atmos. Environ.* **2024**, *321*, No. 120349.
(51) Stein, A. F.; Draxler, R. R.; Rolph, G. D.; Stunder, B. J. B.; Cohen, M. D.; Ngan, F. NOAA's HYSPLIT Atmospheric Transport and Dispersion Modeling System. *Bulletin of the American Meteorological Society* **2015**, *96* (12), 2059−2077.
(52) Liu, R.; Liu, T.; Huang, X.; Ren, C.; Wang, L.; Niu, G.; Yu, C.; Zhang, Y.; Wang, J.; Qi, X.; Nie, W.; Chi, X.; Ding, A. Characteristics and Sources of Atmospheric Ammonia at the SORPES Station in the Western Yangtze River Delta of China. *Atmos. Environ.* **2024**, *318*, No. 120234.
(53) Liu, Y.; Nie, W.; Xu, Z.; Wang, T.; Wang, R.; Li, Y.; Wang, L.; Chi, X.; Ding, A. Semi-Quantitative Understanding of Source Contribution to Nitrous Acid (HONO) Based on 1 Year of Continuous Observation at the SORPES Station in Eastern China. *Atmospheric Chemistry and Physics* **2019**, *19* (20), 13289−13308.
(54) *China National Environmental Monitoring Centre Homepage*. https://www.cnemc.cn/ (accessed 2024−06−29).
(55) Mladenova, I.; Lakshmi, V.; Jackson, T. J.; Walker, J. P.; Merlin, O.; de Jeu, R. A. M. Validation of AMSR-E Soil Moisture Using L-Band Airborne Radiometer Data from National Airborne Field Experiment 2006. *Remote Sensing of Environment* **2011**, *115* (8), 2096−2103.
(56) Hersbach, H.; Bell, B.; Berrisford, P.; Hirahara, S.; Horányi, A.; Muñoz-Sabater, J.; Nicolas, J.; Peubey, C.; Radu, R.; Schepers, D.; Simmons, A.; Soci, C.; Abdalla, S.; Abellan, X.; Balsamo, G.; Bechtold, P.; Biavati, G.; Bidlot, J.; Bonavita, M.; De Chiara, G.; Dahlgren, P.; Dee, D.; Diamantakis, M.; Dragani, R.; Flemming, J.; Forbes, R.; Fuentes, M.; Geer, A.; Haimberger, L.; Healy, S.; Hogan, R. J.; Hólm, E.; Janisková, M.; Keeley, S.; Laloyaux, P.; Lopez, P.; Lupu, C.; Radnoti, G.; de Rosnay, P.; Rozum, I.; Vamborg, F.; Villaume, S.; Thépaut, J.-N. The ERA5 Global Reanalysis. *Quarterly Journal of the Royal Meteorological Society* **2020**, *146* (730), 1999−2049.
(57) Dong, X.; Lai, X.; Wang, Y.; Dong, W.; Zhu, J.; Dong, L.; Cen, S. Applicability Evaluation of Multiple Sets of Soil Moisture Data on the Tibetan Plateau. *Front. Earth Sci.* **2022**, *10*, 1−18.
(58) Jägermeyr, J.; Müller, C.; Minoli, S.; Ray, D.; Siebert, S. *GGCMI Phase 3 Crop Calendar*, 2021. https://zenodo.org/records/5062513 (accessed 2024−05−26).
(59) Huo, K.; Ruan, Y.; Fan, H.; Guo, C.; Cai, H. Spatial-Temporal Variation Characteristics of Cultivated Land and Controlling Factors in the Yangtze River Delta Region of China. *Front. Environ. Sci.* **2022**, *10*, 1−18.
(60) Qiu, B.; Hu, X.; Chen, C.; Tang, Z.; Yang, P.; Zhu, X.; Yan, C.; Jian, Z. Maps of Cropping Patterns in China during 2015−2021. *Sci. Data* **2022**, *9* (1), 479.
(61) Yu, X.; Shen, L.; Hou, X.; Yuan, L.; Pan, Y.; An, J.; Yan, S. High-Resolution Anthropogenic Ammonia Emission Inventory for the Yangtze River Delta. *China. Chemosphere* **2020**, *251*, No. 126342.
(62) Zang, Y.; Qiu, Y.; Chen, X.; Chen, J.; Yang, W.; Liu, Y.; Peng, L.; Shen, M.; Cao, X. Mapping Rapeseed in China during 2017−2021 Using Sentinel Data: An Automated Approach Integrating Rule-Based Sample Generation and a One-Class Classifier (RSG-OC). *GIScience Remote Sens.* **2023**, *60* (1), 2163576.
(63) Xu, W.; Zhang, L.; Liu, X. A Database of Atmospheric Nitrogen Concentration and Deposition from the Nationwide Monitoring Network in China. *Sci. Data* **2019**, *6* (1), 51.
(64) Xia, W.; Zhou, W.; Liang, G.; Wang, X.; Sun, J.; Li, S. Study on ammonia volatilization loss from nitrogen fertilizer in the rice-wheat rotation system under optimized nitrogen application. *J. Plant Nutr. Fert.* **2010**, *16* (1), 6−13.
(65) Liu, L.; Cao, Y.; Tian, Y.; Yin, B.; Zhu, Z. Study on soil ammonia volatilization and nitric oxide emissions during the winter wheat season in the Taihu region. *J. Plant Nutr. Fert.* **2013**, *19* (6), 1420−1427.
(66) Crop sowing guideline *the Ministry of Agriculture and Rural Affairs*. http://zdscxx.moa.gov.cn:8080/nyb/pc/calendar.jsp (accessed 2023−12−20).
(67) Evangeliou, N.; Balkanski, Y.; Eckhardt, S.; Cozic, A.; Van Damme, M.; Coheur, P.-F.; Clarisse, L.; Shephard, M. W.; Cady-Pereira, K. E.; Hauglustaine, D. 10-Year Satellite-Constrained Fluxes of Ammonia Improve Performance of Chemistry Transport Models. *Atmospheric Chemistry and Physics* **2021**, *21* (6), 4431−4451.
(68) Liu, P.; Xue, C.; Ye, C.; Liu, C.; Zhang, C.; Wang, J.; Zhang, Y.; Liu, J.; Mu, Y. The Lack of HONO Measurement May Affect the Accurate Diagnosis of Ozone Production Sensitivity. *ACS Environ. Au* **2023**, *3* (1), 18−23.
(69) Zhao, M.; Tian, Y.; Zhang, M.; Yao, Y.; Yin, B.; Zhu, Z. Reducing NH3 and NO emissions from rice-wheat rotation in the Taihu region through improved agronomic management practices. *Soil* **2015**, *47* (5), 836−841.

https://doi.org/10.1021/acs.est.4c12324
Environ. Sci. Technol. 2025, 59, 5119−5130

(70) Ali, M.; Haruna, A. O.; Majid, N. M. A.; Primus, W. C.; Maikol, N.; Asap, A.; Naharuddin, A. N.; Jeffary, A. V. Using Soil Water to Control Ammonia Emission from Acid Soils with and Without Chicken Litter Biochar. *SAR* **2019**, *8* (3), 23.
(71) Farquhar', G. D.; Firth, P. M.; Wetselaar, R.; Weir, B. On the Gaseous Exchange of Anunonia between Leaves and the Environment: Determination of the Ammonia Compensation Point. *Plant Physiol.* **1980**, *66* (4), 710−714.
(72) Baobin, H.; Peng, C.; Yihang, Y. The characteristics of soil HONO emission and emission factors after fertilization. *Acta Sci. Circumstantiae* **2021**, *42* (8), 449−458.
(73) *Determining_limiting_and_excess_regents_1.Pdf*. https://www.uah.edu/images/administrative/student-success-center/resources/handouts/handouts_2019/determining_limiting_and_excess_regents_1.pdf (accessed 2024−06−23).
(74) Zhao, Y.; Yuan, M.; Huang, X.; Chen, F.; Zhang, J. Quantification and Evaluation of Atmospheric Ammonia Emissions with Different Methods: A Case Study for the Yangtze River Delta Region, China. *Atmospheric Chemistry and Physics* **2020**, *20* (7), 4275−4294.
(75) Wang, T.; Liu, M.; Liu, M.; Song, Y.; Xu, Z.; Shang, F.; Huang, X.; Liao, W.; Wang, W.; Ge, M.; Cao, J.; Hu, J.; Tang, G.; Pan, Y.; Hu, M.; Zhu, T. Sulfate Formation Apportionment during Winter Haze Events in North China. *Environ. Sci. Technol.* **2022**, *56* (12), 7771−7778.
(76) Liu, M.; Song, Y.; Zhou, T.; Xu, Z.; Yan, C.; Zheng, M.; Wu, Z.; Hu, M.; Wu, Y.; Zhu, T. Fine Particle pH during Severe Haze Episodes in Northern China. *Geophys. Res. Lett.* **2017**, *44* (10), 5213−5221.
(77) Mumford, M. T.; Rowlings, D. W.; Scheer, C.; De Rosa, D.; Grace, P. R. Effect of Irrigation Scheduling on Nitrous Oxide Emissions in Intensively Managed Pastures. *Agriculture, Ecosystems & Environment* **2019**, *272*, 126−134.
(78) Guo, X.; Drury, C. F.; Yang, X.; Daniel Reynolds, W.; Fan, R. The Extent of Soil Drying and Rewetting Affects Nitrous Oxide Emissions, Denitrification, and Nitrogen Mineralization. *Soil Science Society of America Journal* **2014**, *78* (1), 194−204.
(79) Fierer, N.; Schimel, J. P. Effects of Drying−Rewetting Frequency on Soil Carbon and Nitrogen Transformations. *Soil Biology and Biochemistry* **2002**, *34* (6), 777−787.

https://doi.org/10.1021/acs.est.4c12324
Environ. Sci. Technol. 2025, 59, 5119−5130